Wave Energy in Space-Time Checkerboard Patterns

Analysis of Electromagnetic Wave Energy in a Medium with Controlled Time-Varying Properties

A Major Qualifying Project submitted to the faculty of

Worcester Polytechnic Institute

In partial fulfillment of the requirements for the degree of Bachelor of Science

by:

Michael A. Perrone (Mathematics),

June 27, 2016
Submitted to:
WPI Advisor: Professor Konstantin Lurie
Sponsor: N/A

Contents

1 Executive Summary **2**

2 Acknowledgements **4**

3 Introduction **5**

3.1 Motivation 5

4 Background **6**

4.1 Electromagnetic Plane Wave in Space-Time Dependent Medium . . . 7

4.2 Reflection and Transmission at Spatial and Temporal Boundaries . . 8

4.3 Wave Energy at Corners in 1+1D Checkerboards 11

5 Methodology **17**

5.1 Wave Energy Density and Energy Flux 18

5.2 Introduction to Clawpack 19

6 Results **20**

6.1 Impedance mismatch in the square checkerboard 21

6.2 Energy Growth from Impedance Mismatch 24

6.3 Impedance Mismatch in Various Checkerboard Geometries 28

7 Discussion **33**

8 Conclusion **36**

9 Future Research **37**

10 Bibliography **39**

List of Figures

1 Derivative discontinuity forms across diagonal characteristic 12

2 Discontinuity amplifies subsequently 15

3 Square checkerboard DM with matched impedance 21

4 Square checkerboard DM with 16.66% impedance mismatch 22

5 Square checkerboard DM with 28.57% impedance mismatch 23

6 Square checkerboard DM with 37.5% impedance mismatch 24

7 Pure temporal laminate 25

8 Temporal laminate with mismatch of both impedance and velocity . . 26

9 Temporal laminate with only impedance mismatch, for differing initial conditions 26

10 Temporal laminate with with 50% impedance mismatch over a 15 temporal periods 27

11 Mismatched impedance for DM checkerboard parameters m=0.55 n=0.5 28

12 Mismatched impedance for DM checkerboard parameters m=0.5 n=0.55 28

13 Matched and mismatched impedance for DM checkerboard parameters m=0.5 n=0.5 29

14 Matched and mismatched impedance for DM checkerboard parameters m=0.6 n=0.6 30

15 Matched and mismatched impedance for DM checkerboard parameters m=0.7 n=0.7 30

16 Matched and mismatched impedance for DM checkerboard parameters m=0.5 n=0.7 31

17 Matched and mismatched impedance for DM checkerboard parameters m=0.7 n=0.5 31

18 Matched and mismatched impedance for DM checkerboard parameters m=0.8 n=0.5 32
19 Matched and mismatched impedance for DM checkerboard parameters m=0.9 n=0.5 32
20 Exchange of energy between left-going and right-going waves only once symmetry is broken. 35

Abstract

Dynamic materials (DM) comprise spatial material frameworks and their energetic interactions with the environment responsible for temporal changes in material properties [7]. Theoretical work has been done to understand DM systems, and now practical means are being developed for the engineering of physical systems. In this paper a checkerboard pattern of variable permeability μ and permittivity ϵ in space-time is studied which permits energy accumulation and concentration in electromagnetic waves travelling through the pattern. Impedance mismatch causes reflection of energy which one would expect to slow energy accumulation, but this does not happen until noticeable impedance mismatch. To explore why this occurs, the exchange of energies of the right-going and left-going families of waves in the DM are tracked over time, and some analysis is performed. Impedance mismatch was found to produce energy accumulation effects separate from those of velocity mismatch. In most of the simulations, these effects more than make up for the losses from reflection out of limit cycles, but some of the simulations suggest parameters exist for which energy loss may occur.

1 Executive Summary

Space-time checkerboard patterns with varying electromagnetic properties ε and μ have been observed to add energy to and increase the frequency of electromagnetic waves travelling through them. Furthermore it has been observed that electromagnetic waves travelling in these dynamic materials may still accumulate energy when the impedance γ is mismatched, causing reflection.

A finite volume method (FVM) wave equation example code from Clawpack 5.4 [6, 1, 10] was modified to simulate electromagnetic wave propagation in a 1+1D checkerboard structure with various impedance mismatches and material parameters m and n corresponding to the sharp checkerboard used in [14]. Initial energy of the wave is separated into the energy associated with left-going and right-going families of characteristics using the energy flux and energy density per volume element. These energies are graphed along with total energy and an approximation of the theoretical limit curve. This allows closer inspection of the effect of impedance mismatch on energy accumulation.

It was found that in a certain range of parameters, impedance mismatch of a checkerboard DM with velocity mismatch adds more energy than it removes by reflection out of limit cycles. The mechanism by which it adds energy was explored, and it was found for example, that due to the symmetric nature of the impedance term in the reflection and transmission coefficients, impedance mismatch could lead to exponential growth even in a pure temporal laminate, and thus outside the generation range found for velocity mismatch by [14]. Preliminary data suggests the generation range for velocity was not substantially decreased size even for noticeable impedance mismatch. Although energy accumulation by velocity mismatch

was quite stable against impedance mismatch, a set of parameters for the DM was found with both impedance mismatch and velocity mismatch but no net growth of energy over time. This case exhibited a lack of exchange of energy or tendency towards equilibrium between the right-going and left-going wave families although their initial values differed and there did not appear to be symmetries to prevent net energy exchange.

2 Acknowledgements

I would like to thank Professor Konstantin Lurie for his guidance with the subject matter, patience with my learning process, and enthusiasm for the project. I would also like to thank William C. Sanguinet for sharing his deep insight into the field of DM and for providing programming assistance.

3 Introduction

Dynamic materials (DM) provide a new perspective for analyzing materials in general. By definition, DM are material assemblies that change their properties in space and time. Temporal change is necessarily accompanied by mass/momentum/energy exchange with the environment [7]. So the DM is *essentially* a union of the material framework and the flux of mass/momentum/energy between it and the environment. This definition means that DM is a thermodynamically open system [7]. It is through DM like muscle tissue that life typically interacts with the environment. This new way of looking at materials promises both the development of a better understanding of biological systems, and the development of practical engineered constructions. This paper analyzes a DM construction in which wave speed and impedance vary in space-time, causing the accumulation of energy and power of electromagnetic waves travelling through the dielectric DM.

3.1 Motivation

A 1+1D transmission line with varying inductance and capacitance in space and time was recently studied [9, 8]. The inductance and capacitance were piecewise constant, taking alternating values within evenly-spaced doubly periodic rectangular regions in 1+1D space-time. This material geometry takes the shape of a checkerboard with spatial and temporal material boundaries. The wave velocities in this DM were alternating, but the wave impedance was kept constant. At spatial boundaries energy flux is preserved; at the temporal boundaries, the energy density changes by the ratio of the wave speed after the transition over the wave speed before it [15, 12, 8]. When this ratio exceeds 1, energy is accumulated and the frequency increases. At the same time, for special ranges of geometric parameters of a checkerboard, waves

tend to concentrate in regions where this ratio exceeds 1 [15]. This concentration brings the wave routes into progressively sharpening beams that approach selected wave routes named stable limit cycles. The energy is accumulated along those wave routes as time is running. In the limit, once the energy supply from the external agent has no bounds, the beams converge to delta pulses carrying infinite energy and infinite power. Unlike a laser which exhibits resonant amplification of energy in a wave by interaction with excitations of the atoms, the DM transmission line exhibits *non-resonant* energy accumulation by interaction with its time varying properties, and power concentration for a wide range of frequencies [9]. Similar DM with accumulation and concentration behaviors could have many practical applications, and thus warrant further study.

4 Background

Dynamic materials, introduced above, are open systems described by a material framework and its energetic interactions with the environment. DM are not in equilibrium: they exchange energy with their environment and therefore are thermodynamically open systems[7]. In general this means that the properties of the material framework may vary in both space and time. Time-independent laminates and composites are in numerous applications, but time variability in properties gives rise to novel physical effects. Property changes may happen without material motion due to the effect of an external agent; such systems are called *activated* DM. An example is given by a piezoelectric structure in a time-varying electric field, causing the material to change shape over time and emit sound. Alternatively, DM may be produced by relative motion of the material fragments. Such DM are called *kinetic*. An example of kinetic DM comes from electrodynamics of moving bodies where

relative mechanical motion is known to affect the constitutive material relations (Minkowskian formulae).

The focus of this paper is an activated DM checkerboard with rectangular regions of constant ε and μ in 1+1D, with sharp transitions to different material properties in adjacent rectangular regions. At the temporal interfaces, the boundary conditions cause changes in frequency and energy of waves travelling in the medium. This energy comes from the work done by an external agent against the electromagnetic wave travelling through the framework during temporal transition. We look to the case of a polarized plane wave propagating in a checkerboard DM, which is simple but allows us to understand the fundamental behaviors of waves in property patterns of higher dimension.

4.1 Electromagnetic Plane Wave in Space-Time Dependent Medium

Electromagnetic plane waves obey the Maxwell's equations:

$$\frac{\partial \overrightarrow{B}}{\partial t} + \nabla \times \overrightarrow{E} = 0, \quad \frac{\partial \overrightarrow{D}}{\partial t} - \nabla \times \overrightarrow{H} = 0, \tag{1}$$

and the material relationships $\overrightarrow{D} = \varepsilon \overrightarrow{E}$ and $\overrightarrow{B} = \mu \overrightarrow{H}$ [4, 2]. The coefficients ε and μ take two different pairs of constant values: (ε_1, μ_1) in material 1, and (ε_2, μ_2) in material 2, alternating in the cells of a DM checkerboard. The model is simplified by assuming a polarized plane wave travelling in the x-direction, with $\overrightarrow{B} = B_3\ \hat{k}$ and $\overrightarrow{D} = D_2\ \hat{j}$, so that

$$(B_3)_t + (\frac{D_2}{\varepsilon})_x = 0, \quad (D_2)_t + (\frac{B_3}{\mu})_x = 0, \tag{2}$$

In the DM checkerboard ε and μ are constant within rectangular regions and jump between constant values at the boundaries between regions. Similarly to the examples in [7], in order to solve for the variable coefficient case, we introduce potentials ϕ and ψ which satisfy

$$(\phi)_x = B_3, \quad (\psi)_x = D_2, \quad -(\phi)_t = \frac{D_2}{\varepsilon}, \quad -(\psi)_t = \frac{B_3}{\mu}. \tag{3}$$

Note that $\phi_{tx} - \phi_{xt} = 0$ and $\psi_{tx} - \psi_{xt} = 0$, obeying equality of mixed partials. We rewrite the system of PDEs in terms of the potentials

$$\psi_t + (\frac{1}{\mu}\phi_x) = 0, \quad \phi_t + (\frac{1}{\varepsilon}\psi_x) = 0, \tag{4}$$

which is a hyperbolic system of conservation laws solvable by Clawpack 5.4 [1, 6, 10], and corresponding to the second order, variable coefficient wave equations

$$(-\varepsilon\phi_t)_t + (\frac{1}{\mu}\phi_x)_x = 0, \quad (-\mu\psi_t)_t + (\frac{1}{\varepsilon}\psi_x)_x = 0, \tag{5}$$

which are easily found by substituting definitions of the potentials into the equalities of mixed partials.

4.2 Reflection and Transmission at Spatial and Temporal Boundaries

For reflection and transmission at a spatial boundary between linear isotropic material regions 1 and 2 of differing ε and μ,

$$[E_{\|}]_1^2 = 0, \quad [H_{\|}]_1^2 = 0, \tag{6}$$

[4, 5]. which for a boundary located at x_0 produces the system of equations

$$E_i e^{(k_1 x_0 - \omega t)} + E_r e^{(-k_1 x_0 - \omega t)} = E_t e^{(k_2 x_0 - \omega t)}, \tag{7}$$

$$\frac{1}{\mu_1 v_1}\left(E_i e^{(k_1 x_0 - \omega t)} - E_r e^{(-k_1 x_0 - \omega t)}\right) = \frac{1}{\mu_2 v_2} E_t e^{(k_2 x_0 - \omega t)}. \tag{8}$$

Where $v_1 = \frac{1}{\sqrt{\mu_1 \varepsilon_1}}$ and $v_2 = \frac{1}{\sqrt{\mu_2 \varepsilon_2}}$ are the *wave speeds* in materials 1 and 2. Note that $H = \pm \frac{1}{\mu v} E$ plus for right-going, and minus for left-going wave. *Frequency* ω of an electromagnetic wave is preserved across the spatial boundary, so that the temporal derivative may be continuous, but for that to hold, the *wave number* k must differ because wave speeds differ. From 7 and 8 reflection and transmission coefficients for electric field can be found:

$$E_r = \frac{1 - (\frac{\mu_1 v_1}{\mu_2 v_2})}{1 + (\frac{\mu_1 v_1}{\mu_2 v_2})} E_i, \quad E_t = \frac{2}{1 + (\frac{\mu_1 v_1}{\mu_2 v_2})} E_i. \tag{9}$$

Reflection and transmission coefficients for energy in terms of electric field,

$$U = \frac{1}{2}(\varepsilon E^2 + \mu H^2) = \varepsilon E^2, \tag{10}$$

are determined completely by the wave impedance $\gamma = \sqrt{\frac{\mu}{\varepsilon}}$ through the formulae

$$R = \frac{U_r}{U_i} = (\frac{\gamma_1 - \gamma_2}{\gamma_1 + \gamma_2})^2, \quad T = \frac{U_t}{U_i} = \frac{\gamma_2}{\gamma_1}(\frac{2\gamma_1}{\gamma_1 + \gamma_2})^2. \tag{11}$$

[3] Note that at a spatial boundary $R + T = 1$, thus energy is conserved. This is not true at a temporal interface where D and B field are continuous instead of E and H. At a sharp temporal switch from material 1 to material 2,

$$[D_\parallel]_1^2 = 0, \quad [B_\parallel]_1^2 = 0. \tag{12}$$

[12] This produces the system of equations for an incident right-going wave

$$\varepsilon_1 E_i e^{(kx-\omega_1 t_0)} = \varepsilon_2 \left(E_r e^{(kx+\omega_2 t_0)} + E_t e^{(kx-\omega_2 t_0)} \right), \tag{13}$$

$$\frac{1}{v_1} E_i e^{(kx-\omega_1 t_0)} = \frac{1}{v_2} \left(-E_r e^{(kx+\omega_2 t_0)} + E_t e^{(kx-\omega_2 t_0)} \right), \tag{14}$$

at time t_0. Note that wave number k is continuous across the temporal interface, but frequency changes due to the difference in wave speed. For the temporal interface, the reflection and transmission coefficients in terms of E then become

$$E_r = \frac{1}{2}(\frac{\varepsilon_1}{\varepsilon_2} - \frac{\sqrt{\mu_1\varepsilon_1}}{\sqrt{\mu_2\varepsilon_2}})E_i, \quad E_t = \frac{1}{2}(\frac{\varepsilon_1}{\varepsilon_2} + \frac{\sqrt{\mu_1\varepsilon_1}}{\sqrt{\mu_2\varepsilon_2}})E_i. \tag{15}$$

[12] Reflection and transmission coefficients of energy at the temporal boundary then take the form

$$T = \frac{U_t}{U_i} = \frac{1}{2}\left[\frac{1}{2}(\frac{\varepsilon_1}{\varepsilon_2} + \frac{\mu_1}{\mu_2}) + \frac{\sqrt{\mu_1\varepsilon_1}}{\sqrt{\mu_2\varepsilon_2}}\right], \tag{16}$$

$$R = \frac{U_r}{U_i} = \frac{1}{2}\left[\frac{1}{2}(\frac{\varepsilon_1}{\varepsilon_2} + \frac{\mu_1}{\mu_2}) - \frac{\sqrt{\mu_1\varepsilon_1}}{\sqrt{\mu_2\varepsilon_2}}\right]. \tag{17}$$

[12] These coefficients can then be expressed in terms of *wave impedance* $\gamma = \sqrt{\frac{\mu}{\varepsilon}}$ and wave speed v (note that $\varepsilon = \frac{1}{\gamma v}$ and $\mu = \frac{\gamma}{v}$)

$$T = \frac{U_t}{U_i} = \frac{1}{2}\left[\frac{1}{2}\frac{v_2}{v_1}(\frac{\gamma_2}{\gamma_1} + \frac{\gamma_1}{\gamma_2}) + \frac{v_2}{v_1}\right] = \frac{1}{2}\frac{v_2}{v_1}\left[\frac{1}{2}(\frac{\gamma_2}{\gamma_1} + \frac{\gamma_1}{\gamma_2}) + 1\right], \tag{18}$$

$$R = \frac{U_r}{U_i} = \frac{1}{2}\left[\frac{1}{2}\frac{v_2}{v_1}(\frac{\gamma_2}{\gamma_1} + \frac{\gamma_1}{\gamma_2}) - \frac{v_2}{v_1}\right] = \frac{1}{2}\frac{v_2}{v_1}\left[\frac{1}{2}(\frac{\gamma_2}{\gamma_1} + \frac{\gamma_1}{\gamma_2}) - 1\right], \tag{19}$$

Expressing the coefficients in this way demonstrates that energy changes at tem-

poral boundaries according to

$$R + T = \frac{U_t + U_r}{U_i} = \frac{1}{2}(\frac{\varepsilon_1}{\varepsilon_2} + \frac{\mu_1}{\mu_2}) = \frac{1}{2}\frac{v_2}{v_1}(\frac{\gamma_2}{\gamma_1} + \frac{\gamma_1}{\gamma_2}). \tag{20}$$

[12] For proper choices of checkerboard geometry and material parameters v and γ, waves will tend to gather in the slow material before each temporal transition, so energy tends to increase. Such choices exist even for surprisingly large impedance mismatch.

It is worth noting that energy remains positive for both the reflected and transmitted wave at the temporal boundary in both right-handed and left-handed materials for which $v_1 > 0, v_2 > 0, \gamma_1 > 0, \gamma_2 > 0$ are real numbers but ε and μ may be both positive or both negative. This is because

$$F = \frac{\gamma_2}{\gamma_1}, \quad \frac{1}{F} = \frac{\gamma_1}{\gamma_2}, \quad \frac{1}{2}\frac{v_2}{v_1}\left[\frac{1}{2}(F + \frac{1}{F}) \pm 1\right] \geq 0, \tag{21}$$

Reflection is zero when $F = \frac{1}{F}$ because this represents the case of matched impedance, but otherwise both reflection and transmission coefficients are positive as expected.

4.3 Wave Energy at Corners in 1+1D Checkerboards

At corners of a 1+1D checkerboard DM, finite jumps in the derivatives of the potentials originate which do not affect energy. To illustrate, consider the case of a DM of matched wave impedance and a square grid $m = n = 0.50$ (see figure 1). Wave speeds in the DM are $a_1 = \frac{n}{m} = 1 \geq a_2$ for material 1 and 2 respectively. 'Diagonal' characteristics which pass from corner to corner exist in material 1 of the material property pattern. The function $f(x - a_1 t)$ is a wave potential which is

initially nonzero in one material region with speed a_1 and continuously differentiable there. According to equations (6) and (12), ϕ and ψ as defined in equation (3) have continuous spatial derivatives across temporal interfaces and continuous temporal derivatives across spatial interfaces. The function f will be assumed to share these properties. Function f propagating through its first corner is shown in the following figure:

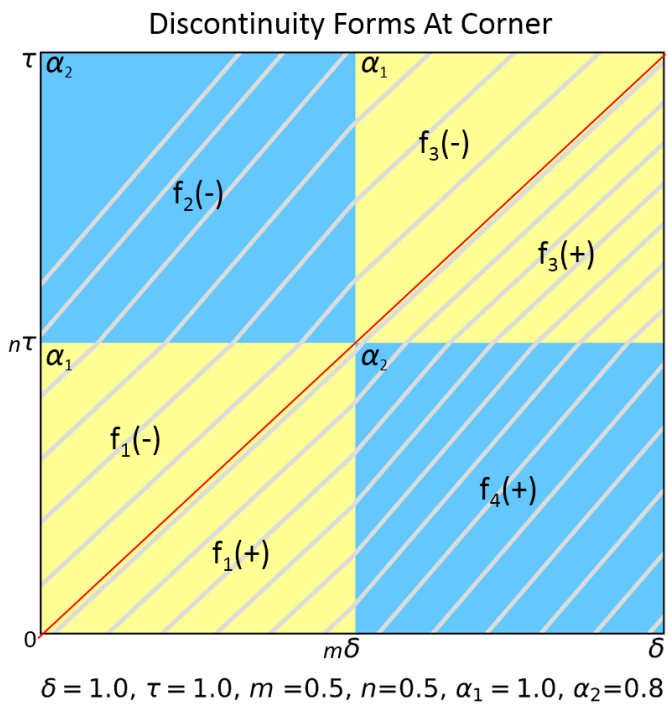

Figure 1: Derivative discontinuity forms across diagonal characteristic

where regions 1 through 4 have wave speeds differing from adjacent regions, and region 1 has speed a_1. $f_n(\pm)$ represents f in each region and specifies whether the argument $x - a_1 t$ is positive or negative in a subset of that region partitioned by the diagonal characteristic, along which $x - a_1 t = 0$ for this example. Because the potential is continuously differentiable across the diagonal characteristic in region 1 we have

$$f_1'(+) = f_1'(-) = f_1'(0). \tag{22}$$

This means that $\lim_{x-at\to 0+} f' = \lim_{x-at\to 0-} f' = C(x,t)$ along the diagonal characteristic in material region 1. Then, as $(m\delta, n\tau)$ is approached along $x - at = 0$, this remains the case so $\lim_{x\to m\delta} \lim_{t\to n\tau} C(x,t) = f_1'(0)$ although continuity no longer holds at the exact point $(m\delta, n\tau)$. For the other boundaries between regions of differing material properties or across other segments of the diagonal characteristic, we have similar equalities. For example,

$$a_1 f_1'(+) = a_2 f_4'(+), \tag{23}$$

which means that along the segment of $(m\delta, t)$, that is the boundary between material regions 1 and 4 not including corner points, $a_1 \lim_{x\to m\delta-0} f' = a_2 \lim_{x\to m\delta+0} f'$ arbitrarily close to $(m\delta, n\tau)$. Additionally,

$$f_1'(-) = f_2'(-), \tag{24}$$

which means that along the segment of $(x, n\tau)$ that is the boundary between material regions 1 and 2 not including corner points, $\lim_{t\to n\tau+0} f' = \lim_{t\to n\tau-0} f'$ arbitrarily close to $(m\delta, n\tau)$. Also,

$$a_2 f_2'(-) = a_1 f_3'(-), \tag{25}$$

which means that along the segment of $(m\delta, t)$ that is the boundary between material regions 2 and 3 not including corner points, $a_2 \lim_{x\to m\delta-0} f' = a_1 \lim_{x\to m\delta+0} f'$ arbitrarily close to $(m\delta, n\tau)$. And finally

$$f_3'(+) = f_4'(+), \tag{26}$$

which means that along the segment of $(x, n\tau)$ that is the boundary between material regions 3 and 4 not including corner points, $\lim_{t\to n\tau+0} f' = \lim_{t\to n\tau-0} f'$ arbitrarily close to $(m\delta, n\tau)$. Thus for a square around the corner $(m\delta, n\tau)$ of side Δx as Δx tends to zero, we can treat the above terms as a system of equations and solve to express f_3' in terms of f_1'. First we use (23) and (26) to find

$$f_1'(0) = \frac{a_2}{a_1} f_4'(+) = \frac{a_2}{a_1} f_3'(+), \tag{27}$$

then we use (24) and (25) to find

$$f_1'(0) = f_2'(-) = \frac{a_1}{a_2} f_3'(-), \tag{28}$$

and using these two new equations we get

$$f_3'(-) = \frac{a_2}{a_1} f_1'(0) = (\frac{a_2}{a_1})^2 f_3'(+), \tag{29}$$

so approaching the diagonal characteristic interface between $f_3'(-)$ and $f_3'(+)$, a jump in derivative limits is introduced which is proportional to $(\frac{a_2}{a_1})^2$. The function f itself remains continuous as long as it was initially continuous, because spatial boundaries require continuity so that the temporal derivative may be continuous, and temporal boundaries require continuity of the spatial derivatives, so a jump in potential cannot be introduced where there was none previously. Since no jumps in the function are present and countably many finite jumps are introduced in its derivative introduced at countably many corner points, the energy integral should be unaffected. This fact does not change if derivative discontinuities travel through

corner points again. To illustrate, consider the next corner point the diagonal characteristic would have gone through from the previous example, (δ, τ). The regions surrounding this point can be represented as

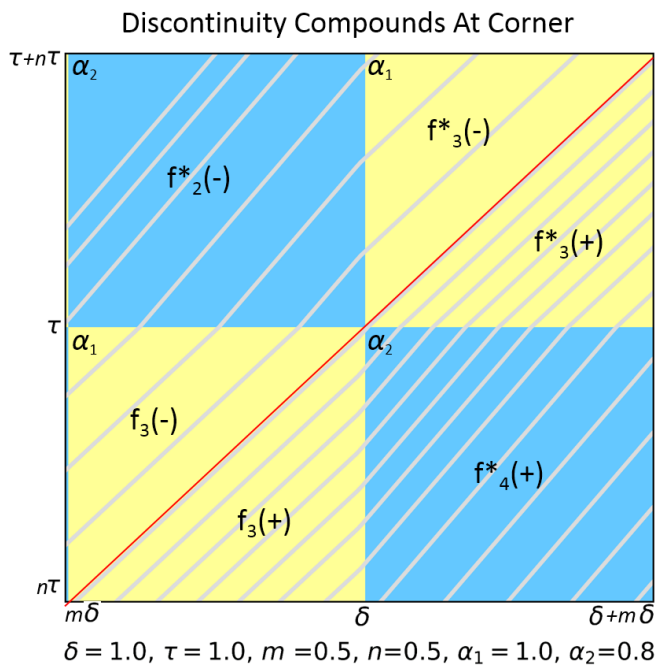

Figure 2: Discontinuity amplifies subsequently

Where the new regions over which potentials are defined are denoted $f*$ and the new region 1* is the old region 3, so we know that along the diagonal characteristic in region 1*, $\frac{a_2}{a_1})^2 \lim_{x-at\to 0+} f'^* = \lim_{x-at\to 0-} f'^*$ which remains true as we approach arbitrarily close to (δ, τ). We can represent this known discontinuity in terms of $f_1'(0)$ using

$$f_1'^*(+) = f_3'(+) = \frac{a_1}{a_2} f_1'(0), \quad f_1'^*(-) = f_3'(-) = \frac{a_2}{a_1} f_1'(0). \tag{30}$$

As in the previous example,

$$a_1 f_1'^*(+) = a_2 f_4'^*(+), \tag{31}$$

which means that along the segment of (δ, t) that is the boundary between material regions 1* and 4* not including corner points, $a_1 \lim_{x\to\delta-0} f' = a_2 \lim_{x\to\delta+0} f'$ arbitrarily close to (δ, τ). Additionally

$$f_1'^*(-) = f_2'^*(-), \tag{32}$$

which means that along the segment of (x, τ) that is the boundary between material regions 1* and 2* not including corner points, $\lim_{t\to\tau+0} f' = \lim_{t\to\tau-0} f'$ arbitrarily close to (δ, τ). Furthermore

$$a_2 f_2'^*(-) = a_1 f_3'^*(-), \tag{33}$$

which means that along the segment of (δ, t) that is the boundary between material regions 2* and 3* not including corner points, $a_2 \lim_{x\to\delta-0} f' = a_1 \lim_{x\to\delta+0} f'$ arbitrarily close to (δ, τ). And finally

$$f_3'^*(+) = f_4'^*(+). \tag{34}$$

which means that along the segment of (x, τ) that is the boundary between material regions 3* and 4* not including corner points, $\lim_{t\to\tau+0} f' = \lim_{t\to\tau-0} f'$ arbitrarily close to (δ, τ). Thus for a square around the corner (δ, τ) of side Δx as Δx tends to zero, we can treat the above terms as a system of equations and put f_3^* in terms of $f_1'(0)$ as

$$f_1'(0) = \frac{a_2}{a_1} f_3'(+) = (\frac{a_2}{a_1})^2 f_4'^*(+) = (\frac{a_2}{a_1})^2 f_3'^*(+), \tag{35}$$

using (31) and (34), and

$$f_1'(0) = \frac{a_1}{a_2} f_3'(-) = \frac{a_1}{a_2} f_2'^*(-) = (\frac{a_1}{a_2})^2 f_3'^*(-), \tag{36}$$

using (32) and (33). With the above two equations we then get

$$f_3'^*(-) = (\frac{a_2}{a_1})^2 f_1'(0) = (\frac{a_2}{a_1})^4 f_3'^*(+). \tag{37}$$

This makes clear that the jump in derivative across $x - a_1 t$ is multiplied by an additional term $(\frac{a_2}{a_1})^2$ after propagation across a second corner region, and is still finite. This should remain true for jumps in derivatives of other finite sizes, as they pass through corner points. Thus there are still countably many finite jumps in derivative, which do not affect energy. When impedance mismatch is introduced it at most doubles the amount of jumps in derivative, which is still countably many, so energy remains unaffected.

5 Methodology

A Finite Volume Method (FVM) is used to simulate a polarized electromagnetic plane wave travelling in a space-time checkerboard DM with differing impedance mismatch and material geometry in each simulation. An FVM was used due to the stability allowed by integral solvers and conservation forms of the wave equation. The FVM solver is the Python package Clawpack, and visualization of the data used various methods. Clawpack allows high-level implementation of FVMs in Python, but allows use of Fortran for fast computation of solutions [6, 1, 10].

5.1 Wave Energy Density and Energy Flux

To study impedance mismatch in a checkerboard DM, the energy of the left-going and right-going families of the wave routes is tracked by decomposing local energy density and local net flux. Poynting vector in the 1+1D checkerboard DM becomes

$$\overrightarrow{S} = S\hat{i} = \overrightarrow{E} \times \overrightarrow{H} = E_2 H_3 \hat{i} = \psi_t \phi_t \hat{i} = \frac{1}{\mu\varepsilon}\psi_x \phi_x \hat{i}. \tag{38}$$

Similarly, local energy density can be expressed as

$$U = \frac{1}{2}(\frac{(\psi_x)^2}{\varepsilon} + \frac{(\phi_x)^2}{\mu}). \tag{39}$$

Spatial derivative approximations are used so that single time steps can be analyzed independently. For an element of the FVM in 1+1D, it is possible to solve for the energy of the left-going and right-going wave families with

$$U_{right} + U_{left} = U, \quad U_{right} - U_{left} = \frac{S}{v}, \tag{40}$$

where the total energy U is the sum of left-going and right-going energy, and the $\hat{i}$ component of the Poynting vector divided by velocity to give units of energy $\frac{S}{v}$ is their difference. This means that for a point x_i at index i in the FVM, the energies for that volume element can be approximated as

$$U_{right}(i) = 0.5 * \left[\frac{1}{2}(\frac{(\frac{\psi_i - \psi_{i+1}}{x_i - x_{i+1}})^2}{\varepsilon_i} + \frac{(\frac{\phi_i - \phi_{i+1}}{x_i - x_{i+1}})^2}{\mu_i}) + \frac{1}{\sqrt{\mu_i \varepsilon_i}} \frac{\psi_i - \psi_{i+1}}{x_i - x_{i+1}} \frac{\phi_i - \phi_{i+1}}{x_i - x_{i+1}}\right], \tag{41}$$

$$U_{left}(i) = 0.5 * \left[\frac{1}{2} \left(\frac{(\frac{\psi_i - \psi_{i+1}}{x_i - x_{i+1}})^2}{\varepsilon_i} + \frac{(\frac{\phi_i - \phi_{i+1}}{x_i - x_{i+1}})^2}{\mu_i} \right) - \frac{1}{\sqrt{\mu_i \varepsilon_i}} \frac{\psi_i - \psi_{i+1}}{x_i - x_{i+1}} \frac{\phi_i - \phi_{i+1}}{x_i - x_{i+1}} \right]. \quad (42)$$

This method introduces error at interfaces where material properties change; this becomes negligible in practice for higher resolution FVMs. Special treatment at boundaries may reduce error in future implementations if additional performance is needed.

5.2 Introduction to Clawpack

The simulations in this paper are run in Clawpack, which is an open-source Python package which uses a finite volume method (FVM) to simulate a system of hyperbolic conservation laws of the form

$$(\kappa(x)q)_t + (f(q, x, t))_x = \psi(q, x, t) \quad (43)$$

in 1+1D, 2+1D or 3+1D [1, 6, 10]. These are called conservation forms because the change over time in the conserved quantities which are elements of the vector q are equal to the flux f entering or leaving the volume element plus any quantity added or removed by the forcing term ψ. Such equations are used in modelling to enforce conservation of energy, momentum, mass, or anything else which should be conserved in a physically realistic simulation. For our electromagnetic simulation we solve the more specific case

$$(q(x, t))_t + (f(q, x, t))_x = 0 \quad (44)$$

Clawpack is given a hyperbolic system of equations of this form as its input. It then iteratively updates a piece-wise constant approximation of the solution of the hyperbolic system by a FVM procedure which guarantees as best it can that the quantities conserved by the physical conservation laws remain conserved in the code. Clawpack uses a Riemann solver to calculate the fluxes of waves through the surfaces of each volume element. It then adds and subtracts all fluxes from their corresponding volume elements to update to the next time step [1, 6, 10]. There are a number of Riemann solvers available in Clawpack and the programmer chooses the one that works best for their system of conservation laws. In this paper riemann.vc_acoustics_2D is used; it still works well for a 1D problem and is built for a problem analogous to the electromagnetic system explored. It is worth noting that the CFL condition for this system implies that the fluctuations must not completely cross a cell or information is lost. Thus $s\delta t < \delta x$ our spatial interval limits our time step. Also worth noting is that for our system $(q(x,t))_t + (f(q,x,t))_x = 0$ the wave speeds are based on the eigenvalues of f'.

6 Results

FVM simulations were performed in Clawpack for varying impedance mismatch, initial conditions, and DM parameters m and n. For each set of parameters, exchange of energy between right-going and left-going wave families was graphed along with total energy and an approximate limit curve for energy growth where applicable. The *limit curve*, as defined in [14], is the theoretical maximum energy growth possible in a checkerboard DM with *matching* wave impedances and differing wave speeds. It increases by the factor $(\frac{v_{fast}}{v_{slow}})^2$ per temporal period. The mesh used by the graphs shown below is comprised of 50 evenly spaced time steps per temporal period (see

small hatch marks on the horizontal axis). Any slight slopes in energy exchange at temporal boundaries are due to this lower resolution when graphing, as the temporal transitions happen instantly in these models. Impedance mismatches are calculated by the difference of the impedances over the larger impedance: $\frac{\gamma_{large}-\gamma_{small}}{\gamma_{large}}$.

6.1 Impedance mismatch in the square checkerboard

The graphs in this section all have initial conditions describing a single right-going wave. As expected for the case of matched impedance, there is no reflected wave and therefore no energy transfer takes place.

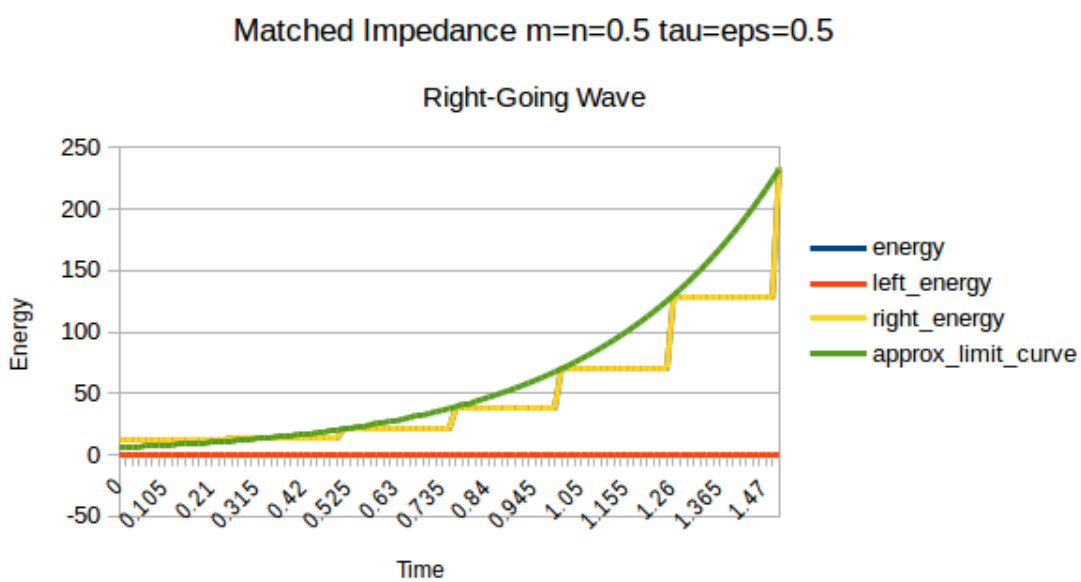

Figure 3: Square checkerboard DM with matched impedance

As impedance mismatch appears, reflection and energy exchange between right- and left-going waves become noticeable, and energy still increases, though there is the potential for decrease because reflected waves may lose energy by leaving the fast material into the slow material through the temporal interface.

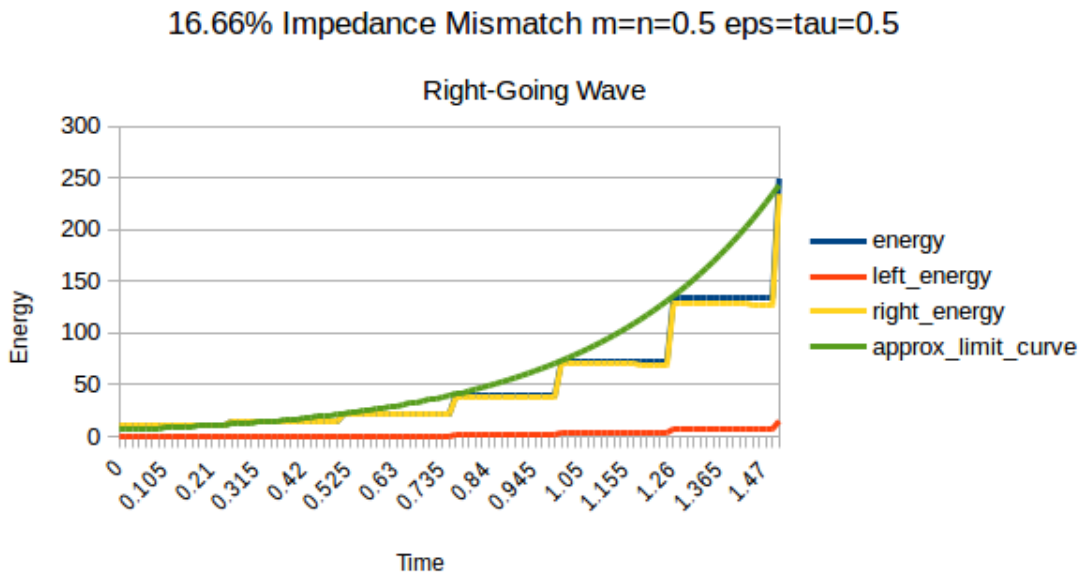

Figure 4: Square checkerboard DM with 16.66% impedance mismatch

In fact energy grows beyond the limit curve describing energy accumulation only due to the velocity pattern, without the impedance mismatch.

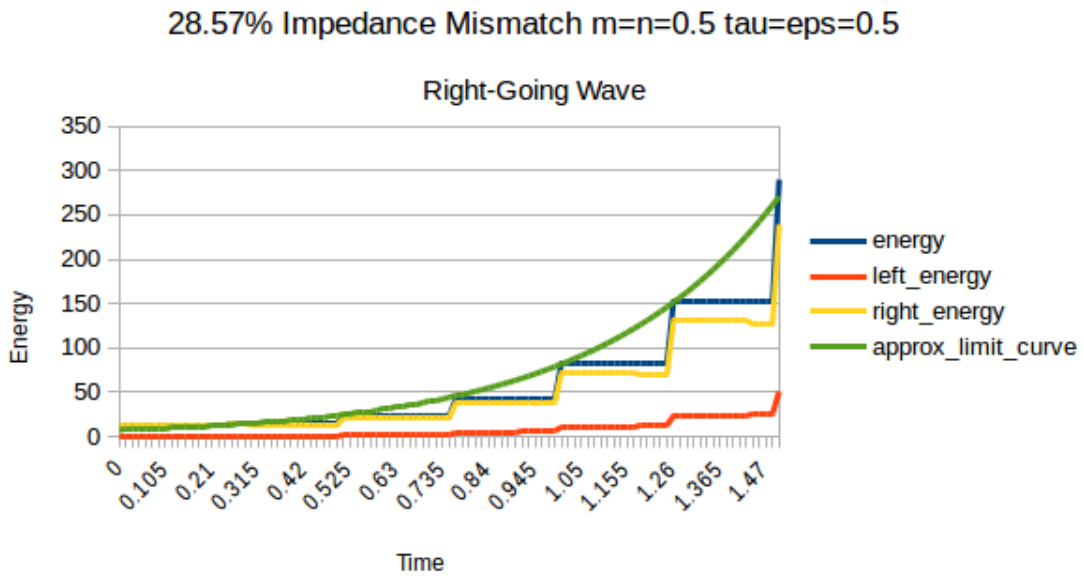

Figure 5: Square checkerboard DM with 28.57% impedance mismatch

As we increase impedance mismatch, the excess energy accumulation seems to occur faster later in the simulation.

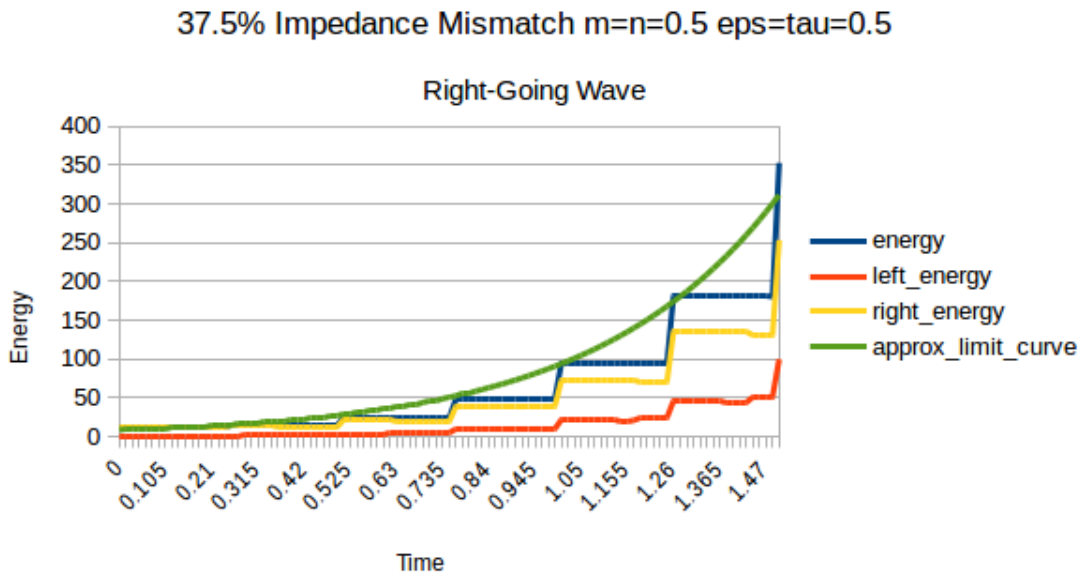

Figure 6: Square checkerboard DM with 37.5% impedance mismatch

6.2 Energy Growth from Impedance Mismatch

The excess energy growth appears due to the effect of impedance mismatch. This is evident in the behavior of purely temporal DM laminates, which may still exhibit energy growth. In a pure temporal laminate without impedance mismatch, no energy growth is observed (see figure 7).

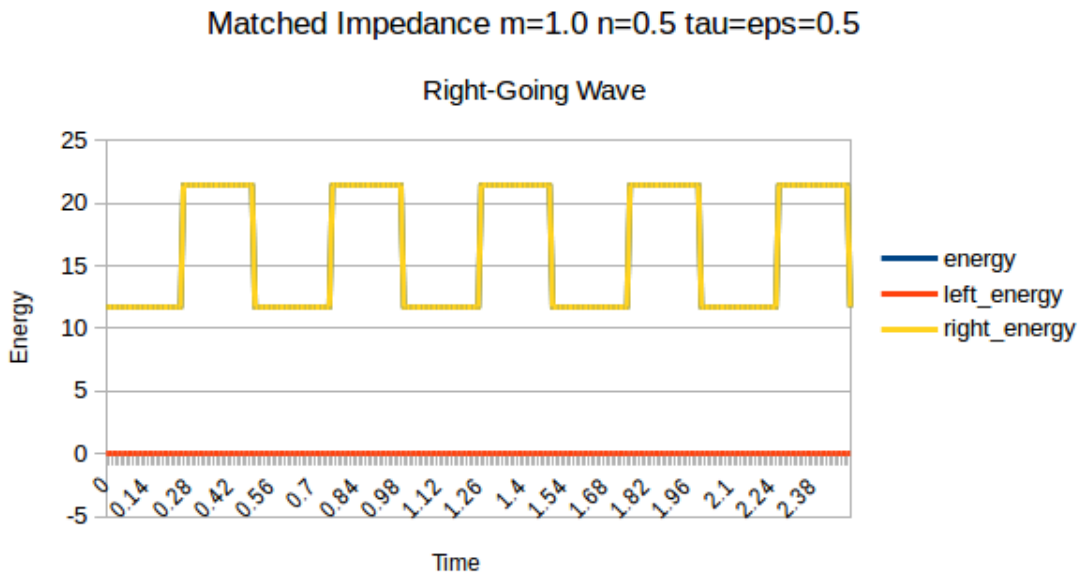

Figure 7: Pure temporal laminate

However, in a temporal laminate with 28.57% impedance mismatch, but also phase velocities of 0.6 and 1.1, some changes in energy over time are visible, but it is unclear whether energy continues to accumulate later on. There also appears to be energy loss at times which may be dependent on the shape of the wave, but it could also be due to a numerical issue. In a temporal laminate with 37.5% impedance mismatch (see figure 8), energy accumulation by impedance mismatch becomes more evident. If there is numerical error, the error eventually becomes small relative to the energy accumulation behavior:

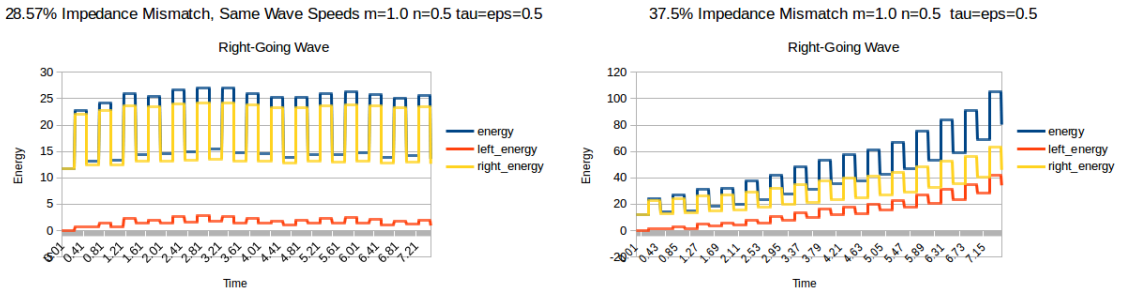

Figure 8: Temporal laminate with mismatch of both impedance and velocity

In figure 8, when total energy increases, both right-going and left-going energies increase, but when total energy is not increasing, left-going and right-going energy remain different and do not have net energy exchange over one temporal period. It should also be mentioned that the initial conditions used in this section all have characteristic wavelengths within an order of magnitude of the product of the temporal period of the laminate, and the wave speed. Other wavelengths for the initial condition may have different energy accumulation or attenuation in the same DM laminate. If wave speeds are matched and impedance varies instead, this growth effect can be isolated from the effects of wave speed:

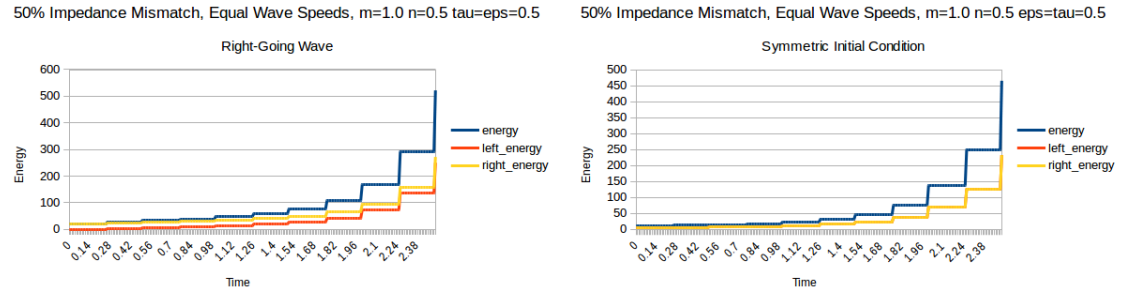

Figure 9: Temporal laminate with only impedance mismatch, for differing initial conditions

The numerical results show that temporal laminates with only impedance mis-

match initially grow slower than expected from the associated energy growth factor (11). The symmetric initial condition also apparently grows faster because it starts out with half of the energy but ends with a similar energy to the example with a right-going initial condition, suggesting that the form of the initial conditions affects the numerical results. It should be explored whether this is purely numerical or has some physical significance. Simulations of temporal laminates with impedance mismatch can be run for many more temporal periods than checkerboard DM with velocity mismatch and material geometry in the generation range:

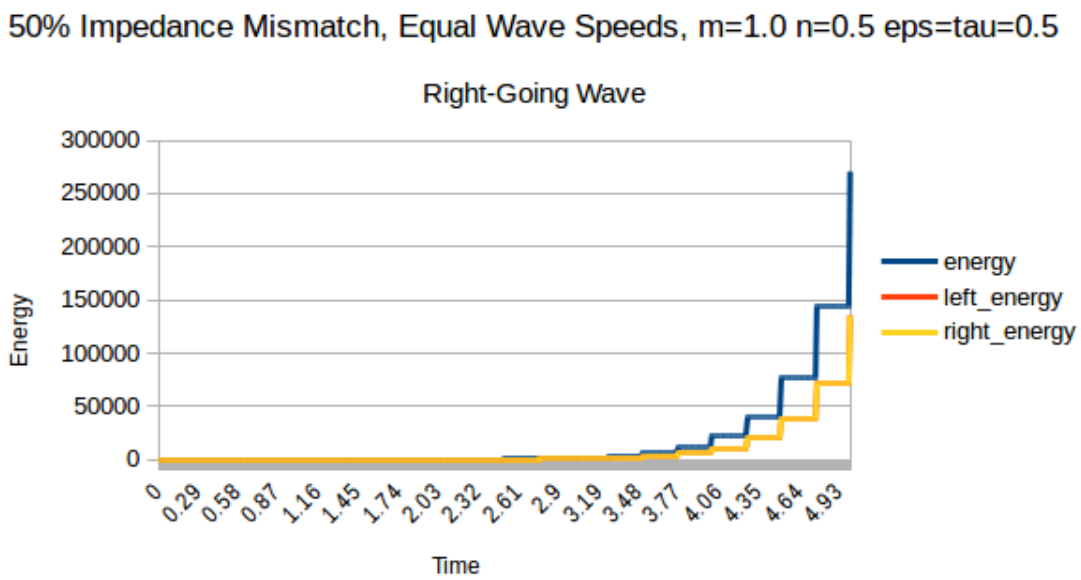

Figure 10: Temporal laminate with with 50% impedance mismatch over a 15 temporal periods

This is because for a temporal laminate with impedance mismatch, energy accumulation happens via a transmission and reflection with greater energy and the same frequency as the initial wave, so frequency does not build towards the resolution limit of the simulation.

6.3 Impedance Mismatch in Various Checkerboard Geometries

For a wide variety of parameters m and n, and even outside the generation range for velocity specified by [14], impedance mismatch leads to energy growth. Impedance mismatches as large as 50% apparently do not change the shape of the generation range for velocity significantly. Inside the generation range, any energy loss from reflection onto paths that will enter the slow material temporally is overcome by the contribution to energy by impedance mismatch at the temporal boundary.

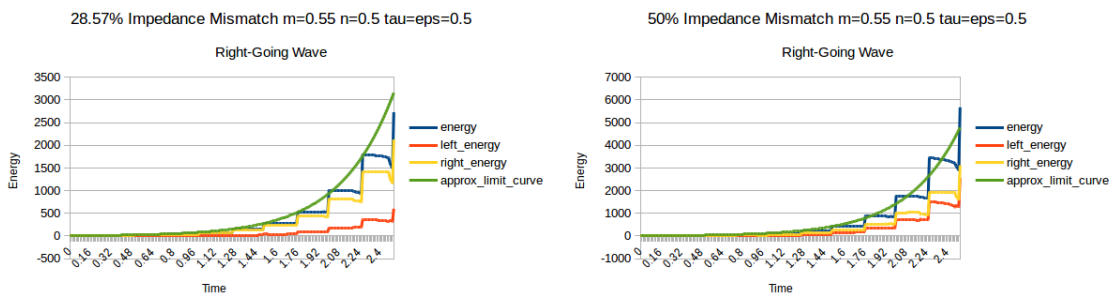

Figure 11: Mismatched impedance for DM checkerboard parameters m=0.55 n=0.5

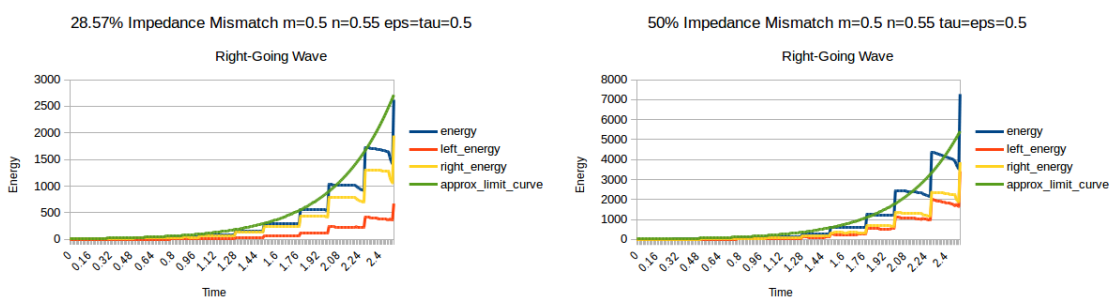

Figure 12: Mismatched impedance for DM checkerboard parameters m=0.5 n=0.55

This is probably because even for 50% impedance mismatch, the reflections induced do not alter the fundamental geometry of the limit cycles towards which

transmitted and reflected characteristics branching from an initial characteristic converge. More simulations should be run to better characterize the size and shape of the generation range with impedance mismatch. It is interesting to note that energy growth from impedance mismatch played a larger role when n was varied than when m was varied, even though impedance mismatch energy accumulation is maximized for a temporal laminate where $m = 1.0, n = 0.5$.

Outside the generation range, the behavior of energy accumulation changes dramatically. Characteristics occasionally focus and accumulate energy when they pass through spatial and temporal interfaces one after the other, but then energy growth stops as they begin entering and leaving two temporal gates consecutively, and finally energy reduces as the characteristics diverge, returning to the start of this cyclic process. This has been observed in [14]. Adding impedance mismatch does not appear to alter this behavior, but it does allow for additional energy accumulation by the mechanism shown in figure 10 which can happen during intervals where temporal laminate behavior is expressed.

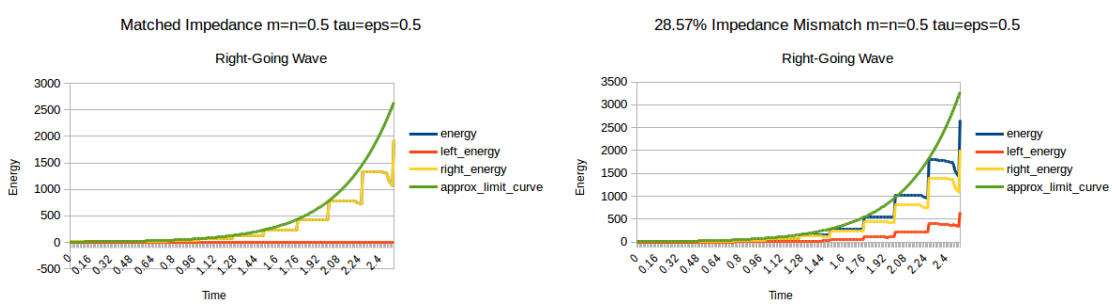

Figure 13: Matched and mismatched impedance for DM checkerboard parameters m=0.5 n=0.5

At the center of the generation range, exponential energy accumulation is noticeable and both impedance and wave speed mismatches contribute to the effect.

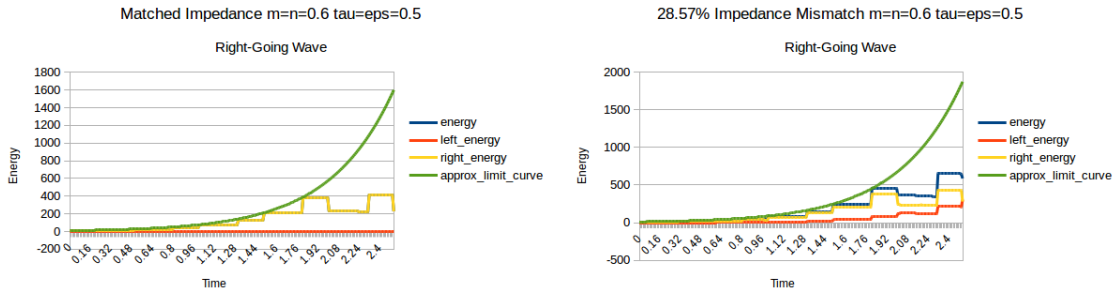

Figure 14: Matched and mismatched impedance for DM checkerboard parameters m=0.6 n=0.6

Slightly outside the generation range, exponential growth occurs for a couple time steps, allowing the wave from the initial condition to sharpen into a pulse. Because the pulse is concentrated enough, all the energy in the pulse follows similar characteristics begins entering two temporal interfaces consecutively, evident by a sharp transition to quasi-temporal laminate behavior. Energy growth still occurs for the case with impedance mismatch.

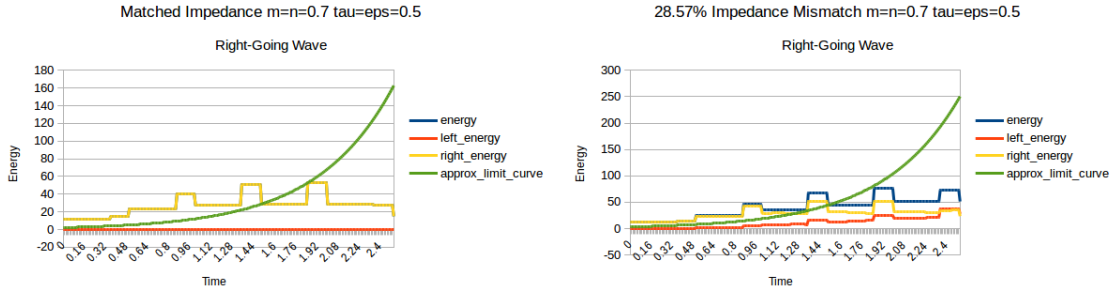

Figure 15: Matched and mismatched impedance for DM checkerboard parameters m=0.7 n=0.7

Further from the generation range, the wave energy accumulates less and quickly transitions to behavior similar to a temporal laminate. Impedance mismatch again adds some energy.

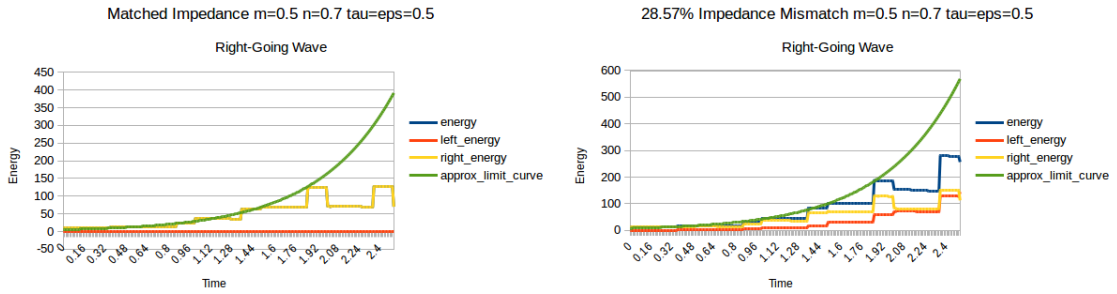

Figure 16: Matched and mismatched impedance for DM checkerboard parameters m=0.5 n=0.7

Outside the generation range, nearer to spatial laminate behavior, less overall energy growth happens. This makes sense because contributions of impedance and velocity to energy accumulation should vanish as a spatial laminate geometry is approached. This is in contrast to inside the generation range, where varying n away from 0.5 appears to aid energy growth more than varying m.

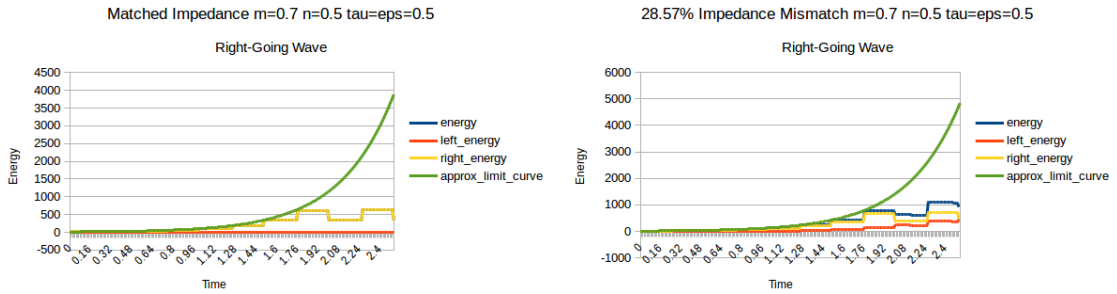

Figure 17: Matched and mismatched impedance for DM checkerboard parameters m=0.7 n=0.5

Moving the same distance toward a temporal laminate in the checkerboard parameter space, energy accumulation is approximately 5 times greater before the transition to temporal laminate behavior. This is because energy growth by impedance mismatch may continue during temporal laminate behavior but vanishes for geome-

tries approaching the spatial lamination.

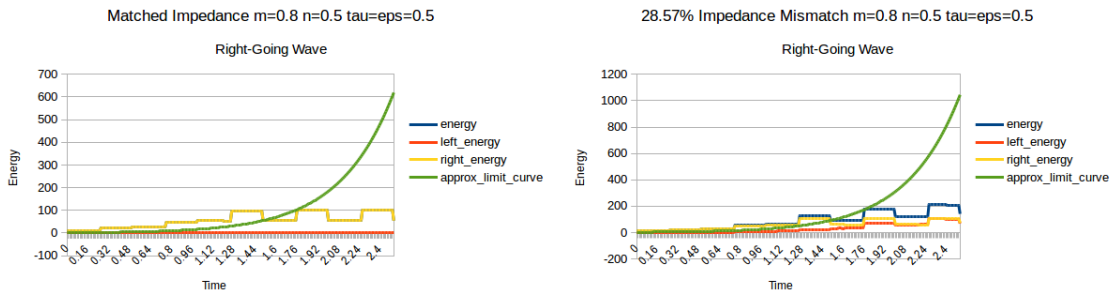

Figure 18: Matched and mismatched impedance for DM checkerboard parameters m=0.8 n=0.5

As the temporal lamination is approached, the wave energy accumulates less, and the transition to temporal laminate behavior begins sooner and occurs over a longer amount of time.

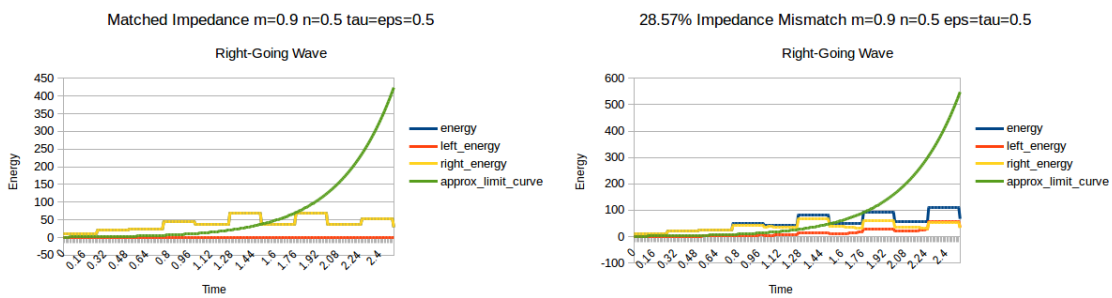

Figure 19: Matched and mismatched impedance for DM checkerboard parameters m=0.9 n=0.5

Even closer to the temporal boundary, energy growth from velocity mismatch becomes very small and the energy behavior becomes very similar to that of a pure temporal laminate. There is still some contribution to energy by impedance mismatch.

7 Discussion

The appearance of energy accumulation by impedance mismatch was initially surprising, but it makes sense in terms of (21) since for equal velocities but mismatched impedances, the coefficient of energy accumulation at the temporal boundary becomes $\frac{(F+\frac{1}{F})}{2} \geq 1$. Unlike velocity mismatch, the sum of the ratios of impedances is symmetric across interfaces in a temporal laminate, so energy growth results in a pure temporal laminate. Delay in the appearance of exponential energy growth (as in figure 9) for temporal laminates with impedance mismatch may be an issue of numerical implementation, or it may be a physical effect due to the violation of some assumption taken when deriving (20). Temporal laminates with only impedance mismatch likely alter amplitudes of reflected and transmitted waves at a temporal boundary while preserving frequency. If it were otherwise, it would not be practical to simulate 10 for the full 15 temporal periods because the frequency of the wave would approach the resolution limit of the simulation.

Over time, spatial periodicity may develop in waves in temporal laminates with impedance mismatch. To illustrate, imagine a temporal laminate with extremely high impedance mismatch for which the transmission and reflection coefficients are approximately equal. Define a factor $\eta = \frac{\frac{\gamma_1}{\gamma_2}+\frac{\gamma_2}{\gamma_1}}{2}$ to be their average. Consider an initial condition which is a spatially symmetric pulse that is solely amplified by impedance mismatch, with an amplitude of 1 and which approaches zero outside a radius from its maximum to a distance of $v\Delta t$ which is the phase velocity v and the temporal period Δt of the temporal laminate. Before the first temporal transition there will be one pulse with a maximum energy density amplitude of 1. Before the following temporal transition, there will be 2 pulses spaced apart by $v\Delta t$ with amplitudes of approximately $1 * \frac{\eta}{2}$ and $1 * \frac{\eta}{2}$. Before the third temporal transition,

there will be three pulses with energy density amplitudes $1*(\frac{\eta}{2})^2$, $4*(\frac{\eta}{2})^2$, and $1*(\frac{\eta}{2})^2$. Before the fourth temporal transition, There will be four groups of Gaussian pulses with amplitudes $1*(\frac{\eta}{2})^3$, $9*(\frac{\eta}{2})^3$, $9*(\frac{\eta}{2})^3$, $1*(\frac{\eta}{2})^3$ and it becomes evident that the peaks of energy density can approximate the squares of the values of Pascal's triangle. More generally the term η may vary if there are families of waves that grow and other families that attenuate in the initial conditions, but many of the spatial periodicities that can form depending on the initial conditions may still share a relationship with Pascal's triangle, perhaps even when their wavelengths are very different from $v\Delta t$.

When there are both velocity and impedance mismatch, energy accumulation is not guaranteed in the simulations. Velocity mismatch and impedance mismatch are each capable of producing energy accumulation on their own in a DM of appropriate geometry, but when they are both present they can compete and reduce the overall effect. It is evident that $\frac{\gamma_1}{\gamma_2} + \frac{\gamma_2}{\gamma_1}$ is maximized as one impedance approaches infinity and the other approaches zero, but are there other local or global maxima once both impedance and velocity vary? There may even be ranges of parameters m, n, γ_1, v_1, γ_2 and v_2 where energy is reduced over time. If such ranges of parameters exist, they would require that energy loss from reflections into regions with unfavorable velocities is greater than energy gain from impedance mismatch and transmission into favorable regions. The idea that impedance mismatch should reduce energy presumes that energy concentrated near limit cycles where reflection would cause it to decrease, but for many DM geometries this may not be accurate. It may be valuable to measure the amount of energy on trajectories along which it will attenuate and compare it to energy on trajectories along which it will accumulate. This can be done by selective space-dependent sums of left-going and right-going energy, dependent on the material geometry. If energy loss can be made exponential

over time in a certain range of parameters, these DM may be used instead of the Perfectly Matched Layer (PML) boundary condition, which exhibits similar behavior in terms of exponential attenuation of energy but can be quite computationally intense.

In most of the figures, net energy exchange between left- and right-going waves meant that eventually the values of left- and right-going energy would converge towards half of the total energy. This happened whether or not we observed exponential growth or temporal laminate behavior, except for the case with 28.57% impedance mismatch in figure 8. In this case, with mismatch in both impedance and velocity in a temporal laminate, it seems reasonable to expect energy accumulation over time, but this does not happen. This unexpected behavior is accompanied by convergence of left-going and right-going energy to very different values. It is possible these unexpected behaviors are related, so by understanding energy exchange we may understand what is different about this system. For a preliminary understanding of energy exchange we can look to the following figure:

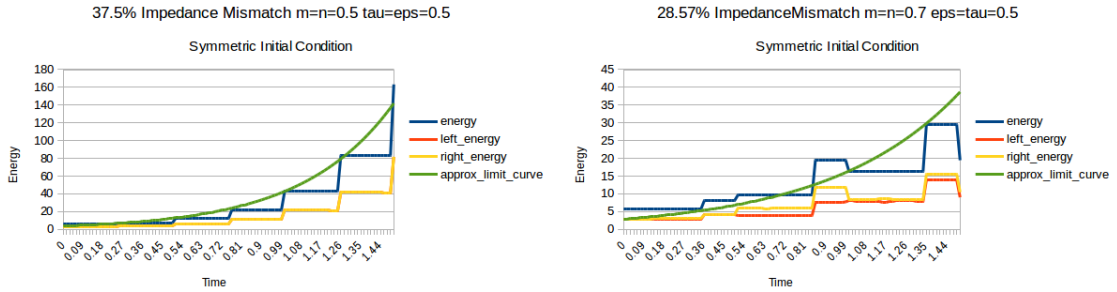

Figure 20: Exchange of energy between left-going and right-going waves only once symmetry is broken.

In figure 20 we see that when the initial conditions share a symmetry with the DM, all reflection and transmission events are balanced by mirror images across the symmetry, and no net energy exchange happens between left- and right-going waves.

When the symmetry is broken, there may be net energy exchange and initially differing energies of left- and right-going waves converge. Thus figure 8 must show a special case where some matching of symmetries or perhaps asymmetries guarantees that no net energy exchange can happen. Perhaps such spaces of parameters for DM can be modeled abstractly with Markov chains.

8 Conclusion

Impedance mismatch in space-time checkerboard DM is not necessarily destructive of energy accumulation, and can even augment it by the energy contribution of impedance mismatch at the temporal boundary. The energy accumulation from impedance mismatch has a larger generation range than that of velocity mismatch found in [14], with accumulation disappearing only as the DM geometry approaches the spatial lamination. Generally speaking, impedance mismatch allows exchange of energy between right-going and left-going waves proportional to the size of the incident waves in the reflection. For example, for an initially right-going wave, right-going energy increases by less than $\frac{v_2}{v_1}$ and left-going energy increases by more, according to how much energy was exchanged by reflection. Thus it is expected that left-going and right-going energy will converge toward equality. Most sets of parameters of the DM behaved this way, but an example was found that does not, and this set of parameters also unexpectedly lacked energy accumulation over time. This hints at the possibility of parameters of the DM for which energy attenuation occurs. The relationship of a special case of the temporal laminate with impedance mismatch to Pascal's triangle underscores the richness of the mathematical field opened by the understanding that impedance mismatch may allow energetic interactions at temporal interfaces as well as velocity.

9 Future Research

Energy growth by impedance mismatch opens up a new and rich avenue of research. Because energy increases via amplitude of the wave instead of frequency (in the absence of wave speed mismatch), it is easier to simulate. Because the temporal laminate where energy growth occurs is simpler than the corresponding checkerboard which allows energy growth under velocity mismatch, energy growth by impedance mismatch may also be easier to implement as a real device. It may be possible to modify the permittivity tensor of a polarizable dielectric through which waves travel by introducing an external electric field. Thus for waves of each particular polarization, the apparent permittivity would change, and the impedance should change accordingly. In this implementation, energy accumulation from impedance mismatch can be thought of as a sort of trapped electron laser as opposed to a free electron laser - where the dipoles of the dielectric material act as driven dipole antennas to add or remove energy from a travelling wave.

If physically meaningful, the odd case of 28.57% impedance mismatch shown in figure 8 suggests some unforseen interaction between velocity mismatch and impedance mismatch for certain geometric parameters of the DM checkerboard, including stabilization of left-going and right-going energies at unequal values, a so far unexplained lack of energy growth, and the possibility of DM parameters for which energy might decrease instead of increasing. All of these possibilities merit further study.

Figure 1 and the surrounding argument about discontinuities introduced at corner points of the checkerboard DM is avoided when taking dispersion into account, according to [11]. It would be interesting to introduce dispersion into the DM checkerboard geometries to observe their effect on the form of limit cycles one ve-

locity becomes frequency dependent. Additionally it may be interesting to explore the behavior of DM checkerboards with absorption or gain; for which μ and ε are complex numbers. In such systems it is not immediately clear whether energy terms will always be positive, so that should be explored analytically.

Another implementation of Clawpack called EMCLAW was developed specifically for electromagnetic simulations in more general cases than what has been explored in this paper [13]. If this software can be utilized instead of just clawpack, future simulations of electromagnetic DM can be done in higher dimensions and in more intricate geometries than just a 1+1D checkerboard laminate.

10 Bibliography

References

[1] Clawpack Development Team. Clawpack software, 2017. Version 5.4.0.

[2] Ian S. Grant and William Robert Phillips. *Electromagnetism*. John Wiley & Sons, 2013.

[3] David J. Griffiths. *Introduction to Electrodynamics*. AAPT, 2005.

[4] David Jeffrey Griffiths and Reed College. *Introduction to electrodynamics*, volume 3. Prentice Hall, Upper Saddle River, NJ, 1999.

[5] Randall J. Jackson. *Classical Electrodynamics*. John Wiley & Sons, second edition, 1962. ISBN 0-471-43132-X.

[6] Randall J. LeVeque. *Finite volume methods for hyperbolic problems*, volume 31. Cambridge University Press, 2002.

[7] Konstantin A. Lurie. *An Introduction to the Mathematical Theory of Dynamic Materials*. Springer Science & Business Media, 2007.

[8] Konstantin A. Lurie, Daniel Onofrei, William C. Sanguinet, Suzanne L. Weekes, and Vadim V. Yakovlev. Energy accumulation in a functionally graded spatial-temporal checkerboard. *IEEE Antennas and Wireless Propagation Letters*, 2016.

[9] Konstantin A. Lurie and Vadim V. Yakovlev. Energy accumulation in waves propagating in space- and time-varying transmission lines. *IEEE Antennas and Wireless Propagation Letters*, PP Issue 99, 2016. ISSN: 1536-1225, DOI: 10.1109/LAWP.2016.2522384.

[10] Kyle T. Mandli, Aron J. Ahmadia, Marsha Berger, Donna Calhoun, David L. George, Yiannis Hadjimichael, David I. Ketcheson, Grady I. Lemoine, and Randall J. LeVeque. Clawpack: building an open source ecosystem for solving hyperbolic pdes. *PeerJ Computer Science*, 2:e68, 2016.

[11] A. V. Maslov and M. I. Bakunov. Reflection and transmission of electromagnetic waves at a temporal boundary: comment. *IRE Transactions on Microwave Theory and Techniques*, 39(20), 2014.

[12] Frederic R. Morgenthaler. Velocity modulation of electromagnetic waves. *IRE Transactions on Microwave Theory and Techniques*, pages 167–172, 1958.

[13] Damian San Roman Alerigi. *Exploring Heterogeneous and Time-Varying Materials for Photonic Applications, Towards Solutions for the Manipulation and Confinement of Light.* PhD thesis, King Abdullah University of Science and Technology, 2014. see http://repository.kaust.edu.sa/kaust/.

[14] William C. Sanguinet. *Various extensions in the theory of dynamic materials with a specific focus on the checkerboard geometry.* PhD thesis, Worcester Polytechnic Institute, 2017.

[15] Yuzhe Xiao, Drew N. Maywar, and Govind P. Agrawal. Reflection and transmission of electromagnetic waves at a temporal boundary. *Optics letters*, 39(3):574–577, 2014.